Desorption Simulation of a Highly Dynamic Metal Hydride Storage System

David Wenger[*1], *Wolfgang Polifke*[*,2], *and Eberhard Schmidt-Ihn*[3]
[1]*Wenger Engineering GmbH*, [2]*Technical University of Munich*, [3]*Daimler AG*
[*]*Wenger Engineering GmbH, Schillerstr. 18, D-89077 Ulm, Germany, mail@wenger-engineering.de*

Abstract: Metal hydrides are a widely-used method for storing and releasing hydrogen chemically under moderate conditions. This paper will present how highly dynamic metal hydride storage has been simulated and optimized using Comsol Multiphysics. It will be shown how mass, energy and momentum balances were implemented and what boundary conditions were set to analyse various scenarios as yet untested in practice. The focus of the work is the simulation of time-variable desorption with high heat source density.

The result of the simulation is an optimized storage system design; with respect to heat transfer, weight and manufacturing outlay. In addition, it can be used to draw conclusions on the optimum storage material for particular requirements.

Keywords: Hydrogen, Metal Hydride, Fuel Cell, Heat- and Mass Transfer.

1 Introduction

Metal hydrides are a widely-used method for storing hydrogen chemically and reversibly. The advantages are moderate pressure (usually much less than 10 MPa) and the possibility for use as hydrogen storage in fuel cells; as heat reservoirs, heat pumps, thermal compressors, hydrogen purifiers or similar. The general chemical reaction is shown by the equation (1):

$$\text{Metal} + \text{H}_2 \leftrightarrow \text{Metal Hydride} + \text{Heat} \quad (1)$$

Typical storage alloys are $LaNi_5$, FeTi, $TiMn_{1.5}$, Mg or new solid storage systems such as alanates, amide/hydride mixtures or boranes [1, 2, 5, 4]. A metal hydride storage system always consists of a pressure vessel, a (sintered metal) filter, a heat transfer medium (e.g. air or water) and perhaps additional components to improve heat transfer. The goal of the simulation presented was to optimize a highly dynamic metal hydride storage system, taking into account a wide range of application scenarios.

2 Mathematical model of a metal hydride storage system

Figure 1 shows the interdependencies in a metal hydride storage system.

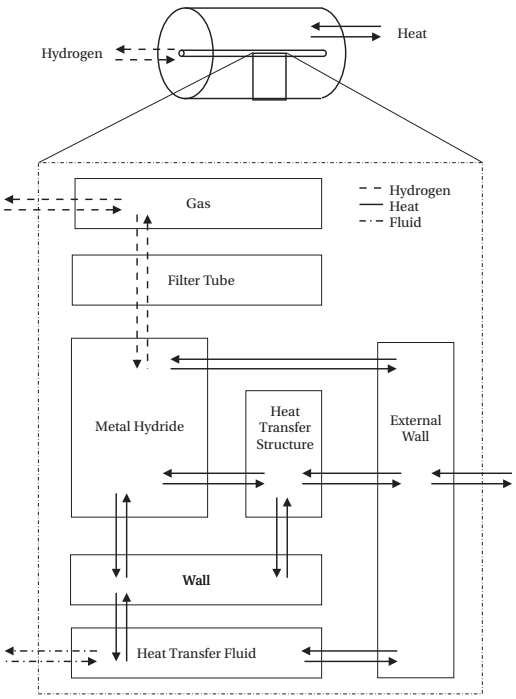

Figure 1: Interdependencies in a metal hydride storage system

The mass, energy and momentum balance in the storage system concerned can be described as follows:

$$\frac{\partial \epsilon\, \rho}{\partial t} = \mathrm{div}(\rho\, \vec{u}) - \dot{\omega}\,, \quad (2)$$

$$\rho \frac{\partial \vec{u}}{\partial t} + \frac{\eta}{\kappa_{MeH}} \vec{u} + \nabla p = \vec{F}\,, \tag{3}$$

$$\left(\left(1-\epsilon\right)\left(\rho_{Me}\, c_{p,\,Me} + \rho_{MeH}\, c_{p,\,MeH}\right) + \right.$$

$$\left. + \epsilon\, \rho_{\mathrm{H_2}}\, c_{p,\,\mathrm{H_2}} \right) \frac{\partial T}{\partial t} = \nabla \cdot \left(\lambda_{\mathit{eff}} \nabla T - \right.$$

$$\left. - \rho_{\mathrm{H_2}}\, c_{p,\,\mathrm{H_2}}\, T\, \vec{u} \right) + \frac{\partial p}{\partial t} + \dot{\omega}\, \Delta_r h\,, \tag{4}$$

$$p\,V = n\,R\,T\,. \tag{5}$$

The source term for the mass is defined by chemical reaction and is often chosen as an empirical equation.

$$\dot{\omega}_{\mathit{Abs}} = k_1(T)\, \ln\left(\frac{p}{p_{\mathit{eq,\,Abs}}(T,\,c)} \right) k_2(c) \tag{6}$$

$$\dot{\omega}_{\mathit{Des}} = k_3(T)\, \ln\left(\frac{p_{\mathit{eq,\,Des}}(T,\,c)}{p} \right) k_4(c) \tag{7}$$

$$\dot{\omega} = \dot{\omega}_{\mathit{Abs}}\left(p > p_{\mathit{eq,\,Abs}}\right) + \dot{\omega}_{\mathit{Des}}\left(p < p_{\mathit{eq,\,Des}}\right) \tag{8}$$

Here the most important parameter is the equilibrium pressure p_{eq}. This depends on the material and must be specified using measurements at various temperatures, pressures and concentrations. Examples of concentration-pressure isotherms are shown in Figure 2.

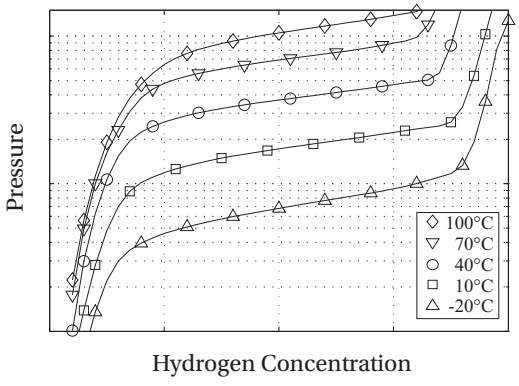

Figure 2: Examples of metal hydride pressure-concentration-isotherms. As there is no precise equation to describe the measured values, these must be included using the interpolation function.

A further important factor is the effective thermal conductivity of the bulk, λ_{eff}. This is often taken as a constant, but actually also depends on the parameters pressure, temperature, concentration and porosity, and material-specific parameters such as alloy construction, particle size distribution, particle form etc. The effective thermal conductivity is very difficult to access experimentally, typical values are in the range of 0.3 .. 1.2 W/m-K. If the bulk is used in a heat transfer matrix, e.g. aluminium foam, effective thermal conductivities of up to 8 W/m-K can be reached. One of the objects of the current simulation was to quantify the influence of the effective thermal conductivity. The start and boundary conditions to be selected can be found using the desired results. During absorption of hydrogen, a constant pressure is applied to the storage system. At first the mass flow in the storage system comes from the pressure gradient ($p_{\mathit{Absorption}} > p_{\mathit{Storage}}$); then the pressure equalizes via the reaction rate. The latter is primarily dependant on the heat dissipated, since the reaction is so fast that chemical equilibrium is reached in a very short time. The situation is different for desorption. Hydrogen is extracted according to consumption, in this case in a fuel cell. The pressure and temperature in the storage system are a result of the complex interaction of the gas mass flow extracted, the heat supplied and the highly non-linear temperature- and pressure-dependant relationships of the material data. In order to portray all processes in the same model, a velocity boundary condition was selected for the in- and outflows. This contained the modelling of the filter using a Darcy equation. The parameter κ_{Filter} must be specified by the filter manufacturer.

$$v_{\mathrm{H_2},\,\mathit{in}} = \frac{\kappa_{\mathit{Filter}}}{\eta\, \delta_{\mathit{Filter}}} \left(p_{\mathit{Abs}} - p_{\mathit{Storage}}\right)\,, \tag{9}$$

$$\dot{m}_{\mathrm{H_2}\,\mathit{in}} = v_{\mathrm{H_2},\,\mathit{in}}\, \rho_{\mathrm{H_2},\,\mathit{in}}\, A\,, \tag{10}$$

$$v_{\mathrm{H_2},\,\mathit{out}} = v_{\mathrm{H_2},\,\mathit{out,\,set}} \times$$
$$\times \left(\dot{m}_{\mathrm{H_2},\,\mathit{out,\,set}} \le \dot{m}_{\mathrm{H_2},\,\mathit{out,\,lim}}\right) +$$
$$+ v_{\mathrm{H_2},\,\mathit{out,\,lim}} \times$$
$$\times \left(\dot{m}_{\mathrm{H_2},\,\mathit{out,\,set}} > \dot{m}_{\mathrm{H_2},\,\mathit{out,\,lim}}\right) \tag{11}$$

with

$$v_{\mathrm{H_2},\,\mathit{out,\,set}} = \frac{\dot{m}_{\mathrm{H_2},\,\mathit{out,\,set}}}{\rho_{\mathrm{H_2}}\, A}\,, \tag{12}$$

$$v_{\mathrm{H_2},\,\mathit{out,\,lim}} = \frac{\kappa_{\mathit{Filter}}}{\eta\, \delta_{\mathit{Filter}}} \left(p_{\mathit{min}} - p_{\mathit{Storage}}\right), \tag{13}$$

$$\dot{m}_{\mathrm{H_2},\,\mathit{out,\,lim}} = v_{\mathrm{H_2},\,\mathit{out}}\, \rho_{\mathrm{H_2}}\, A\,. \tag{14}$$

For the case of outflowing gas, at the start of the test a reference mass flow exits

the container and towards the end, when the storage system pressure is approaching the residual pressure p_{min}, the mass flow is limited by the filter until eventually no more mass flow exits. Using scalable equations, boundary integration variables and Boolean variables, the equations have been constructed in such a way that only one boundary condition is able to cover all cases.

The in- and outflowing enthalpies are linked directly to this using a Neumann boundary condition:

$$\dot{H}_{in} = \dot{m}_{in}\, h_{in} = \dot{m}_{in}\, c_p\, T_{in} \quad (15)$$

$$\dot{H}_{out} = \dot{m}_{out}\, h_{out} = \dot{m}_{out}\, c_p\, T_{Storage} \quad (16)$$

At the heat transferring walls:

$$\dot{Q} = k_i\, A\, \Delta T\,. \quad (17)$$

The values for α_i can be calculated and applied using established scalable relationships from the literature.

For the rest of the boundary conditions, either symmetry, isolation or the no-slip-condition is valid. One pressure and one temperature were selected as starting conditions. A starting concentration c_{Me} and c_{MeH} and a porosity can be found from this by interpolating the PCI.

The domain modeled is shown in Figure 3

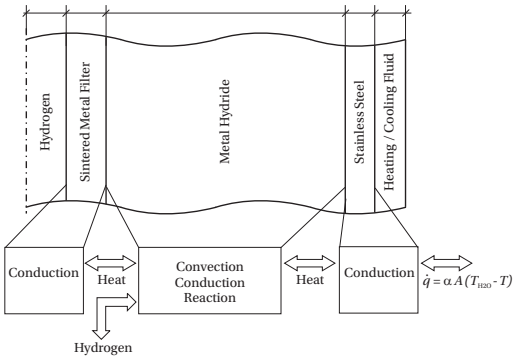

Figure 3: Representation of the area modelled.

3 Validation of the simulation

The simulation is validated by several plausibility calculations and comparison with the measurement data. This way it can be confirmed that both the implementation and the choice of the imprecisely known parameters are correct.

3.1 End temperature in the adiabatic compression of gas

If an adiabatic container, which at the start of the procedure contains an ideal diatomic gas with the pressure p_1 and the temperature T_1, is filled to pressure p_2, an analytical solution can be found for the end temperature T_2. If the temperature of the inflowing gas T_{in} is the same as the starting temperature T_1, then according to [3]:

$$T_2 = T_1 \frac{\kappa}{1 + \frac{p_1}{p_2}(\kappa - 1)} \quad (18)$$

Interestingly, during filling to a very high pressure, the temperature T_2 approaches the limit value

$$\lim_{p_2 \to \infty} \frac{T_2}{T_1} = \kappa\,. \quad (19)$$

So an ideal diatomic gas with $\kappa \approx 1.4$ can heat itself from room temperature to a maximum of 145°C.

The implemented model was used to solve this process for various end pressures and the results compared with the analytical solution according to Equation 18 (Figure 1). No difference can be detected between the analytical solution and the simulation.

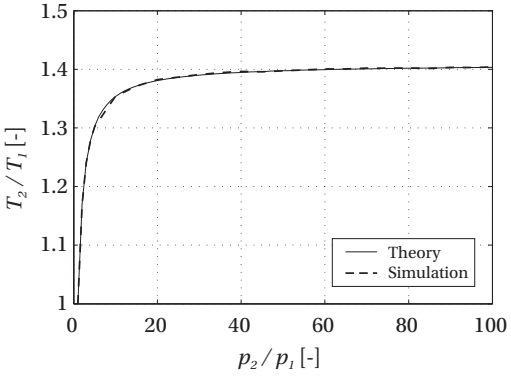

Figure 1: Adiabatic compression of an ideal gas: Comparison of the simulation with the analytical solution

3.2 Heating the bulk without a reaction

The heat transfer and thermal conductivity coefficients in this system can be quantified by heating the storage system at ambient pressure and recording the temperature inside the bulk. The latter is compared with the simulation. The most imprecisely known parameters – $\alpha_{MeH\text{-}W}$ and λ_{eff} – are investigated more closely using a sensitivity analysis and quantified for the boundary conditions present.

Comparison of the heating tests with the simulation. A very good correlation was determined for $\lambda_{eff} = 0.43\,\mathrm{W/m\text{-}K}$.

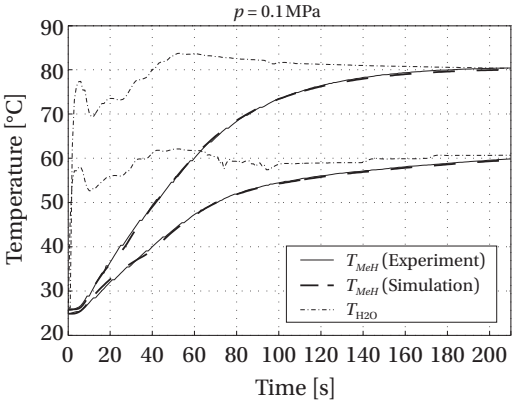

Figure 2: Comparison of the heating tests with the simulation. A very good correlation was determined for $\lambda_{eff} = 0.43\,\mathrm{W/m\text{-}K}$.

Figure 2 shows the results of the comparison. It is clear that the simulation matches the measurements almost perfectly.

3.3 Characteristics of the significant measurement values during desorption

Here a desorption simulation is shown as an example and compared with the corresponding experiment (Figure 3).

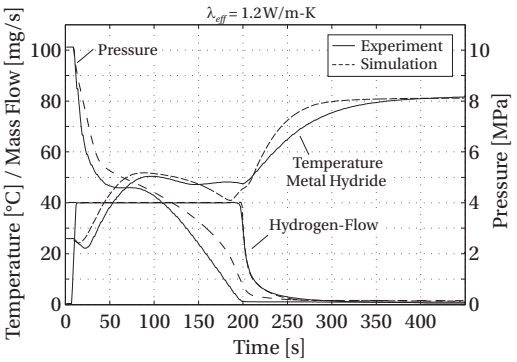

Figure 3: Comparison of a desorption experiment with the simulation (λ_{eff} = 1.2 W/m-K)

By definition, the computed value of the mass flow setpoint agrees with the experiment. That the mass flow starts to decrease at exactly the same point in time emphasises the quality of the simulation. The pressure characteristic is somewhat flatter in the simulation and does not show the distinctive plateau between 50 and 100 seconds. However, the minimum system pressure is reached at the same moment as in the experiment. Although the temperature increases more quickly at the start of the simulation, at the end of the desorption phase it sinks again by around 10 K - an effect which is not shown at all in the experiment. Also, in the last section - where nothing more is being desorbed - the temperature increases significantly faster than in the experiment.

As for absorption, the reasons for these deviations could be inconsistent parameters – the simulation was carried out with e.g. $\lambda_{eff} = const. = 1.2\,\mathrm{W/m\text{-}K}$ – or unaccounted for effects. On the one hand, the thermal warm-up due to the dead time heating the storage system could have an effect; on the other hand, longitudinal effects such as slightly decreasing heating water temperature over the length of the storage system could also play their part.

All in all, the significant effects - the agreement of the hydrogen mass flow and the good approximation of the pressure and temperature characteristics - are reproduced with sufficient accuracy for the model to be used for further simulations.

4 Simulation results

Numerous simulations were carried out to optimize the storage system geometry and to quantify the influence of only imprecisely known parameters (e.g. thermal conductivity) or freely chosen parameters (e.g. equilibrium pressure which can be set using alloy composition). A plot of results is shown here as an example (Figure 1). The maximum value for hydrogen extraction corresponds to an integral heat source density of

$$\dot{q}_{grav} = \frac{\dot{m}\,\Delta_r h}{M_{M,\mathrm{H_2}}\,m_{MeH}} = 2.58\,\mathrm{kW/kg_{MeH}} \quad (20)$$

$$\dot{q}_{vol} = \frac{\dot{m}\,\Delta_r h\,\epsilon\,\rho_{MeH}}{M_{M,\mathrm{H_2}}\,m_{MeH}} = 8.26\times10^3\,\mathrm{kW/m^3_{MeH}} \quad (21)$$

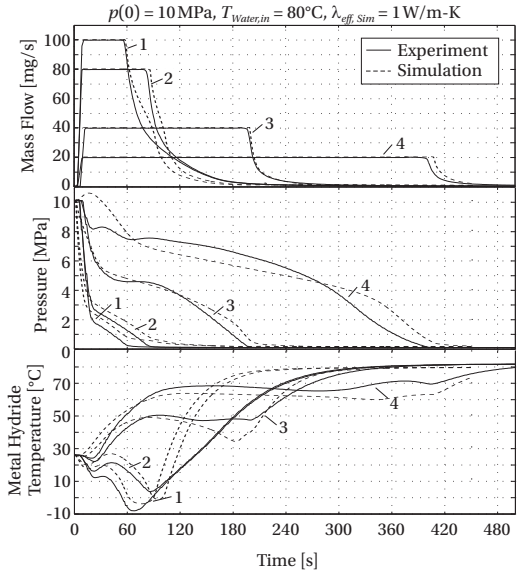

Figure 1: Mass flow, pressure and hydride temperature at various extraction rates.

Simulation shows a good correlation with the experiments. The largest deviation occurs when the storage system is (almost) empty and is at ambient pressure. This is due to the assumption of a constant effective thermal conductivity of 1 W/m-K. But for the conditions present, a value of 0.43 W/m-K would be more appropriate, as shown in Figure 2. However, this deviation can be accepted since this part of the experiment is not so important for the fundamental evaluation.

A further deviation is that in the simulation, the heat is applied immediately at the start of the simulation, but this is not possible experimentally. Due to the valve switching time and the pump warm-up time, a delay occurs leading to a slight temperature and therefore pressure increase at the start. This deviation can be seen particularly clearly in Test 4, where the simulation leads to a pressure increase due to hydrogen desorption in the first few seconds. However, these deviations do not have a significant influence on the hydrogen mass flow. If however the pressures and temperatures need to be reproduced more accurately, the heat capacity flows and their exact temperatures can be incorporated into the simulation using the interpolation function.

The simulation also permits specification of the time variation for the required mass flow. The pressure and temperature in the bulk result from the corresponding extraction rate and the heat supply. If the storage system is empty or the pressure sinks to the minimum storage system pressure, the extraction flow is automatically reduced to zero. Figure 2 shows an example of this kind of variable hydrogen extraction at constant heat capacity flow outside the storage system.

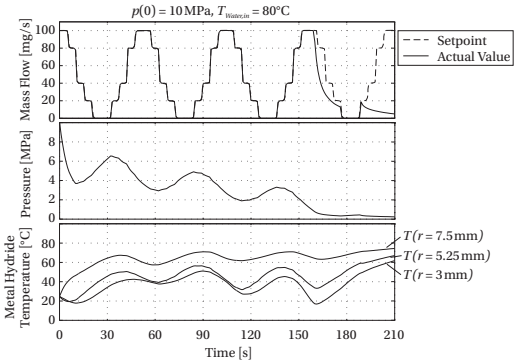

Figure 2: Mass flow, pressure and hydride temperature with time-variable hydrogen extraction.

The required mass flow is maintained perfectly until t = 160 s. Through the constant temperature outside the storage system, a variable heat flow is set up in the storage system, resulting in a periodically increasing and then decreasing pressure. The temperature at various points across the bulk radius also varies. After t = 160 s the storage system is mostly empty and the

pressure ambient. The requested cycle is cancelled automatically.

Figure 3 shows the temperature and concentration profile across the radius in a storage system with a larger radius. The required mass flow has been scaled so that the heat source density is the same as in the tests with 80 and 40 mg/s described above.

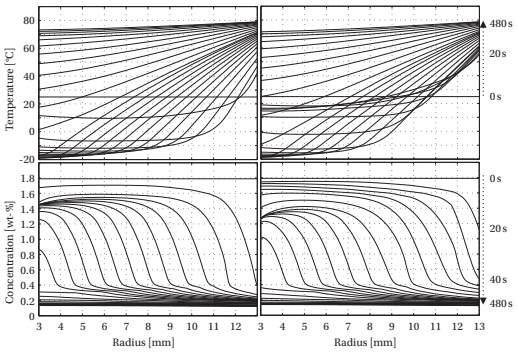

Figure 3: Temperature and concentration profiles across the radius for extraction rates of 270 mg/s (left) and 135 mg/s (right).

Very steep temperature and concentration gradients can be seen. The temperature on the outer edge of the bulk increases continuously towards the water temperature, while the temperature on the inner edge sinks below 0°C in the first minutes. The concentration gradients are also correspondingly steep: while the concentration at the outer edge has already almost reached the minimum after a very short time, at the inner edge it remains at significantly more than 1.3 wt-% for a long time. The reason for this behaviour is the poor thermal conductivity of the bulk powder.

5 Conclusion

This simulation allows absorption and desorption to be calculated in the same model run. The model is independent of artificially selected starting and boundary conditions and is therefore valid over a wide range. Each parameter can be implemented either as a constant, as a scalable equation or via the interpolation of measurement data. Using the Matlab interface, parameter studies can be calculated and output automatically.

Using the simulation, a metal hydride storage system could be thermically optimized in such a way that the required dynamics were achieved without it becoming too difficult for the application.

References

[1] Otto Bernauer, Johannes Töpler, Dag Noreus, R. Hempelmann, and D. Richter, *Fundamentals and properties of some ti/mn based laves phase hydrides*, International Journal of Hydrogen Energy **14** (1989), no. 3, 187–200.

[2] Borislav Bogdanovic and Manfred Schwickardi, *Ti-doped alkali metal aluminium hydrides as potential novel reversible hydrogen storage materials*, Journal of Alloys and Compounds **253-254** (1997), 1–9.

[3] Günther Cerbe and Hans-Joachim Hoffmann, *Einführung in die thermodynamik*, 13. auflage ed., Carl Hanser Verlag, München, 2002.

[4] J. J. Vajo, S. L. Skeith, and F. Mertens, *Reversible storage of hydrogen in destabilized libh4*, Journal of Physical Chemistry B **109** (2005), no. 9, 3719–3722.

[5] Z. T. Xiong, J. J. Hu, G. T. Wu, P. Chen, W. F. Luo, K. Gross, and J. Wang, *Thermodynamic and kinetic investigations of the hydrogen storage in the li-mg-n-h system*, Journal of Alloys and Compounds **398** (2005), no. 1-2, 235–239.